Journal of Pharmacokinetics and Pharmacodynamics (2019) 46:457–472
https://doi.org/10.1007/s10928-019-09649-0

ORIGINALPAPER

A physiologically-motivated model of cystic fibrosis liquid and solute transport dynamics across primary human nasal epithelia

Florencio Serrano Castillo[1] · Carol A. Bertrand[2] · Michael M. Myerburg[3] · Monica E. Shapiro[1] · Timothy E. Corcoran[1,3,4] · Robert S. Parker[1,4,5]

Received: 22 March 2019 / Accepted: 2 August 2019 / Published online: 7 September 2019

Abstract

Cystic fibrosis (CF) disease is caused by mutations affecting the gene coding for the cystic fibrosis transmembrane conductance regulator (CFTR), an anion channel expressed in the mucosal side of epithelial tissue. In the airway, dysfunctional CFTR results in a transepithelial osmotic imbalance leading to hyperabsorption of airway surface liquid mucostasis, chronic inflammation, and eventual respiratory failure. Human nasal epithelial cell cultures from healthy and CF donors were used to perform studies of liquid and solute transport dynamics at an air/liquid interface in order to emulate the in vivo airway. Then, these results were used to inform a quantitative systems pharmacology model of airway epithelium describing electrically and chemically driven transcellular ionic transport, contributions of both convective and diffusive paracellular solute transport, and osmotically driven transepithelial water dynamics. Model predictions showed CF cultures, relative to non-CF ones, have increased apical and basolateral water permeabilities, and increase paracellular permeability and transepithelial chemical driving force for a radiolabeled tracer used to track small molecule absorption. These results provide a computational platform to better understand and probe the mechanisms behind the liquid hyperabsorption and small molecule retention profiles observed in the CF airway.

Keywords Cystic fibrosis · CFTR · Quantitative systems pharmacology · Human nasal epithelial · Airway surface liquid layer · Electrophysiology

Introduction

Cystic fibrosis (CF) is a life-shortening, autosomal recessive disease caused by mutations in the cystic fibrosis transmembrane conductance regulator (CFTR) gene. CF is the most common lethal genetic disorder among Caucasians and occurs at a rate of 1 in every 3400 births in the United States affecting approximately 70,000 patients worldwide [1]. The CFTR gene codes for an anion channel (also referred to as CFTR) expressed on the mucosal side of the epithelium of multiple organ systems, including the pancreas, intestine, reproductive organs, and airways [2]. Loss of CFTR expression or function results in an osmotic imbalance due to defective ion transport. In the respiratory tract, these conditions cause airway surface liquid (ASL) hyperabsorption, mucus dehydration, and depressed mucociliary clearance (MCC). Mucostasis leads to chronic infection and a sustained and unregulated inflammatory response that causes bronchiectasis premature and respiratory failure, the leading cause of CF mortality [2–6].

Electronic supplementary material The online version of this article (https://doi.org/10.1007/s10928-019-09649-0) contains supplementary material, which is available to authorized users.

✉ Robert S. Parker
rparker@pitt.edu

[1] Department of Chemical and Petroleum Engineering, University of Pittsburgh, 940 Benedum Hall, Pittsburgh, PA 15261, USA

[2] Department of Pediatrics, University of Pittsburgh, Pittsburgh, PA, USA

[3] Division of Pulmonary, Allergy, and Critical Care Medicine, University of Pittsburgh, Pittsburgh, PA, USA

[4] Department of Bioengineering, University of Pittsburgh, Pittsburgh, PA, USA

[5] McGowan Institute for Regenerative Medicine, University of Pittsburgh, Pittsburgh, PA, USA

Fundamentally, CF is a disease driven by dysregulation of transepithelial ion and water transport. In healthy epithelia, water, ions, and other solutes are transported across the epithelium via paracellular and transcellular mechanisms [7]. Water transport is primarily driven by osmotic forces across tight junctions or through water channels on the plasma membrane of epithelial cells [8]. Ions and some small molecules are transported transcellularly through active or passive fluxes linked to a multitude of ion channels and cotransporters [9]. Solute transport also occurs in the paracellular space, and it is mediated by both diffusive and convective transport [10]. Cl^-, Na^+, and K^+ concentrations are the main determinants of ASL and cellular volume regulation [7, 11]. In CF, deficient or absent CFTR causes decreased Cl^- and HCO_3^- secretion [4, 12]. In CF, dysfunctional CFTR or its downstream physiological effects have been shown to either directly or indirectly disrupt the normal functions of multiple known members of the epithelial electrophysiology network, including the epithelial sodium channel (ENaC) [13], the solute carrier family 26 member 9 (SLC26A9) [14], the large conductance Ca^{2+} activated K^+ channel (BKCa) [15], aquaporin 3 (AQP3) [16, 17], and some gap and tight junction proteins [18, 19]. The combined effect of these disruptions leads to a homeostatic imbalance that favors the hyperabsorption of ASL.

Electrophysiological measurements are taken using an Ussing Chamber (UC) to study ion and liquid transport dynamics at the airway epithelium. The UC allows for the measurement of the whole-membrane, transepithelial short-circuit current, which provides a direct link to ion transport dynamics under conditions where the epithelium interfaces two static, relatively infinite liquid and ion reservoirs. This technique has been particularly useful in CF, where UC recordings are commonly used to study disease pathophysiology and assess the efficacy of novel CFTR modulators [14, 20, 21]. Several mathematical models have been published that explore the electrophysiological dynamics of the airway epithelium under conditions similar to those of the UC, where apical liquid volume far exceeds physiological conditions. These models have either focused on general descriptions of airway epithelia function [22–24] or explored possible functional differences between CF and non-CF cell cultures [25, 26]. However, the ASL has a much smaller volume under physiological conditions and is often described as a highly dynamic, thin-film volume responsible for epithelial hydration. Thus the conditions assumed in these previous models may limit their applicability to predict ASL dynamics under physiological, or "thin film" conditions, or those associated with ASL dehydration, a hallmark of CF pathophysiology [3, 5, 6, 27]. More recently, Sandefur et al. published an extended model that accounts for thin-film conditions of the airway and includes cellular regulation through both Ca^{2+} and purinergic signals over a physiologically-relevant time period [28]. However, it does not account for all paracellular transport mechanisms or provide a meaningful and scalable metric to extrapolate model predictions to clinical measurements.

Here we present a detailed model characterizing the pathways for liquid and solute transport within the CF airway. The model is informed with data generated from primary human nasal epithelial (HNE) cell cultures harvested from subjects who performed concurrent airway function tests. Contributions of both convective and diffusive paracellular transport on epithelial dynamics are described. In particular, the model includes expressions to track the transport of the radiopharmaceutical Technetium 99m-Diethylenetriamine Pentaacetic Acid (Tc-DTPA), an in vitro analogue of the in vivo functional imaging probe Indium 111-DTPA (In-DTPA), which is used to measure small molecule absorption across the airway epithelium [10]. Radiolabeled DTPA can only move through the paracellular pathway, and its absorption rate characterizes paracellular flows and tight junction integrity. Radiolabeled DTPA absorption is increased in the lungs of patients with CF [5, 10, 27], and in primary human bronchial epithelial (HBE) CF cell cultures where it is strongly correlated with ASL absorption [10]. Functional imaging scans measuring In-DTPA absorption were developed with the goal of detecting changes in liquid absorption in the CF airway—a key indication of therapeutic efficacy.

These types of in vitro to in vivo relations are of particular relevance in the study of CF. Primary cell cultures have played an unusually important role in therapeutic development within this disease, which lacks an easily accessible, reliable animal model that can recapitulate human airway physiology, disease pathogenesis, and the genotypic variety observed in humans [29, 30]. Biophysically-inspired computational models can further facilitate this process by providing a physiologically-grounded bridge between novel cell culture based experimental measurements and commonly used clinical indicators of CF pathophysiology and therapeutic efficacy. The work presented here, an in silico model that leverages knowledge obtained from a parallel assessment of cell and organ level physiology, serves as a first step in this direction. On a longer timeframe, this can yield a platform where in vitro measurements sets can be used to informed data-driven, validated in silico model and generate patient-tailored and phenotype-based analyses of this trans-scale disease.

Materials and methods

Cell culture

HNE cells, collected under a protocol approved by the University of Pittsburgh Institutional Review Board (clinicaltrial.gov number NCT02947126), were cultured from samples obtained from minimally-invasive nasal brushings of donors. Donors either had no history of lung disease and who were not carriers of the 144 most common CFTR mutations associated with CF disease, or had a genetically-confirmed CF diagnosis. In brief, cells were expanded using conditionally reprogrammed cells, allowing for their passaging without loss of quality decline [31, 32]. Following sufficient expansion (80–90% confluency), the cells were seeded onto 0.33 cm^2 filters (0.4 μm pore size, Corning- Costar Transwell® Collagen T-cols, Acton, MA, USA). After 24 h, apical media was removed, and cell cultures were maintained at an air–liquid interface (ALI) thereafter. Basolateral media was changed 3 times weekly. Filters were maintained for at least 4 weeks under ALI conditions and demonstrated active cilia, an indicator of successful epithelial differentiation, before testing [31]. For more detailed information about the cell culture protocol see Online Resource. This study used filters cultured from primary HNE cells from CF (9 subjects, n = 36 filters) and non-CF donors (14 subjects, n = 48 filters) (Table 1).

In vitro ASL and paracellular transport clearance studies

ASL volume and Tc-DTPA apical retention were measured during the 24 h following the addition of 0.01 mCi/ml Tc-DTPA in 10 μL of isotonic Ringer's solution (IR) (115 mM NaCl, 25 mM $NaHCO_3$, 5 mM KCl, 10 mM HEPES, 1 mM $MgCl_2$, 1.5 mM $CaCl_2$, and 5 mM glucose) to the apical surface of the HNE cell cultures. Tc-DTPA radioactivity was measured in the ASL and cell layer by removing the filter from the media and briefly placing it in a well counter. Results were decay and background corrected, normalized by starting counts, and fitted to exponential curves to generate clearance rates [6, 10]. Plates containing HNE cells cultures were imaged with an optical scanner (Epson V500, Epson Corporation, Long Beach, CA, USA). ASL volume was measured using a previously described optical method [33]. These images were then analyzed using an image analysis algorithm implemented in ImageJ (https://imagej.nih.gov/ij/, NIH, Bethesda, MD, USA) [33]. The algorithm utilizes the radial refraction patterns induced as transmitted light passes through the meniscus of the ASL layer to predict a liquid volume from an experimentally determined calibration curve. A diagram detailing the experimental setup for these studies can be found in Fig. 1a. In order to explore the behavior of HNE cell cultures under osmotic stimuli, these studies were also performed following the apical addition of Tc-DTPA in 10 μL of hypertonic Ringer's solution (isotonic + 200 mM NaCl) (HR).

Model structure and development

Based on the model schematic in Fig. 1b, we have developed a system of ordinary differential equations (ODEs) governing liquid and solute transport in HNE cell cultures. HNE cultures are grown at an ALI to mimic physiological conditions in the human airway as closely as possible. In order to accurately describe the dynamic behavior of this system, three compartments are included: (1) the cellular (C) compartment, which accounts for the total intracellular volume across the entire epithelial monolayer (∼ 0.5–1.5 μL); (2) the apical (Ap) compartment consisting of the naturally occurring ASL (∼ 0–25 μL); and (3) the larger basolateral (Bl) compartment, which contains cell culture media (∼ 400 μL). These compartments interface each other in the transport of water, electrolytes, and other solutes through a complex network of ion channels, transporters, and junction proteins across both the paracellular and transcellular pathways [9]. The model includes mathematical expressions characterizing the different transport mechanisms of water, Na^+, Cl^-, K^+, and Tc-DTPA between all three compartments, as well as the electrical potential across both the apical and basolateral membranes. A compartmental description of the model fluxes and compartments can be found in Fig. 2.

The model describes the geometry and dimensions of HNE cell cultures based on the assumption that they are composed of cell monolayers, with individual cells having the shape of rectangular prisms adjacent to one another over the entire filter plane. Accordingly, the model definitions of effective surface area for all tight junctions (A_{TJ}), and apical (A_{Ap}) and basolateral (A_{Bl}) membranes are as follows: A_{TJ} is taken to be the cross-sectional area of the total filter area (A_F = 0.33 cm^2) occupied by tight junctions. A_{Ap} is the remaining area of A_F once A_{TJ} is subtracted. Lastly, A_{Bl} is taken to include both the basal reflection of A_{Ap} and the lateral membrane lining the paracellular space, starting immediately below the tight junctions. Previous work from our lab has shown that when the number of cells in a filter is sufficiently large (as is the case in fully differentiated cell cultures with physiologically-meaningful transepithelial resistance) [34], the following relationship exists:

$$A_{TJ} = A_F \frac{2A_{TJ,1}}{A_{C,1}} \quad (1)$$

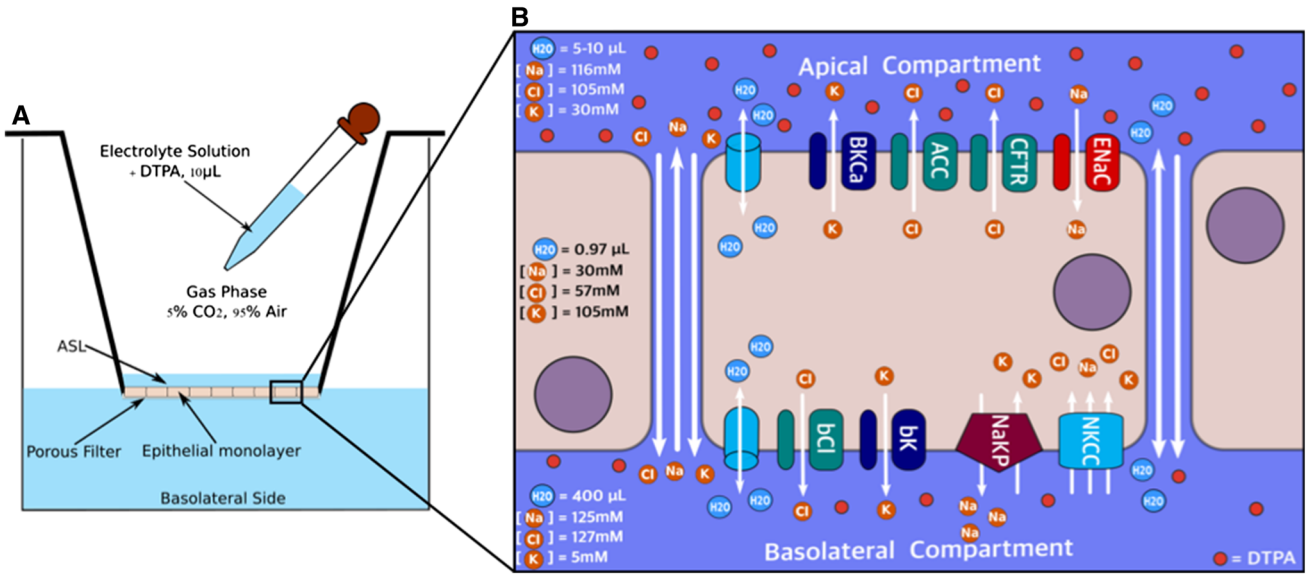

Fig. 1 **a** Schematic of human nasal epithelial (HNE) cell culture experimental conditions. The HNE membrane was seeded and allowed to differentiate on porous supports in the presence of epithelial differentiation media (basolateral side) and a 5% CO_2/95% O_2 gas mixture (Apical side). Membranes naturally develop an ASL volume. At the beginning of the experiments, 10 µL of Ringers solution and Tc-DTPA were added. Tc-DTPA retention (in counts) and ASL volume (in µL) were measured at 0, 2, 4, 6, 8, 12, 24 h following the volumetric stimulus. The zoomed area **b** shows the major contributors to solute and liquid transport across the airway epithelium represented in the model equations. Cellular volume and electrolyte concentrations dynamically respond to changes in electroosmotic driving forces (ion channels) and facilitated ion transport (co-transporters). The model also includes paracellular transport of solutes (ions and Tc-DTPA) through both diffusion and convection, and osmotically driven water flux through both the trans- and paracellular pathways

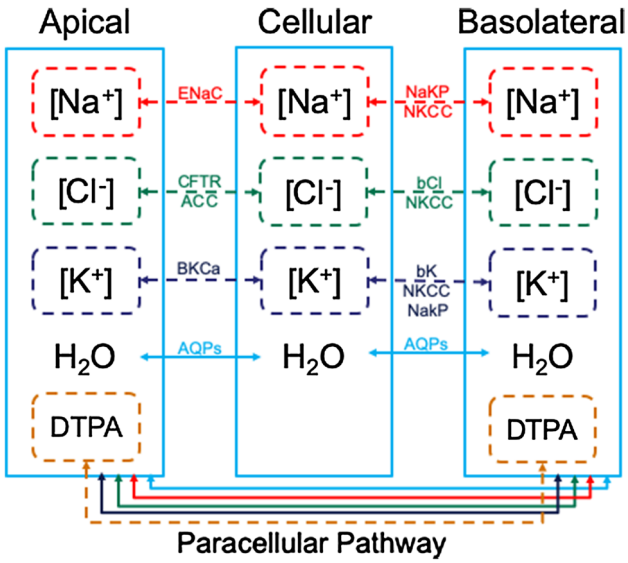

Fig. 2 Compartmental model diagram that highlights the different pathways that affect transcellular and paracellular solute and fluid transport. Model allows for the apical, basolateral, and cellular volume and electrolyte concentrations to dynamically respond to changes in electroosmotic driving forces (ion channels) and facilitated ion transport (co-transporters). The model also includes paracellular transport of solutes (ions and Tc-DTPA) through both diffusion and convection, and osmotically driven water flux through both the trans- and paracellular pathways

Here $A_{TJ,I}$ and $A_{C,I}$ are the areas of a single tight junction section and cell, respectively, calculated from tight junctions cross-sectional length (average separation between two individual cells, L_{TJ} = 60 nm) and a single cell average square face length (L_C= 8 µm) [34]. Initial monolayer volume (V_c) was estimated from cell height (h_c) predictions under the aforementioned geometrical basis and assuming constant total epithelial membrane area [24, 28]. However, V_c, and thus h_c, vary dynamically in response to volumetric and osmotic effects, allowing the monolayer to regulate cellular solute concentration and membrane polarization in response to stimuli [35]. In order to model this behavior, the transport of water between any two compartments ($i \rightarrow j$) is driven solely by osmotic pressure difference, $\Delta\pi_{i,j}$, as described in Eq. 2.

$$\Delta\pi_{i,j} = \sum_k \gamma_k \frac{n_{k,i}}{V_i} - \sum_k \gamma_k \frac{n_{k,j}}{V_j} \quad (2)$$

In this expression, $n_{k,i}$ is the number of moles of solute, k, which is divided by the volume of compartment i and multiplied by osmotic coefficient γ_k. Volume changes in all compartments can thus be caused by water transport across the paracellular pathway, or either of the epithelial membranes, and can be described as:

$$\frac{dV_i}{dt} = V_m \sum_{i,j \neq i} \left(P^w_{i,j} \Delta \pi_{i,j} \right) \tag{3}$$

Here, i refers to any of the three compartments, $P^w_{i,j}$ is the water permeability between compartment i and j, and V_M is the molar volume of water (0.018 L/mol).

The model accounts for the transport of both ionic (Na^+, Cl^-, K^+) and uncharged (Tc-DTPA) solutes. Tc-DTPA can only move between the Ap and Bl compartments through the paracellular space. All ionic solutes can move both paracellularly and transcellularly. In transcellular flux, ion transport can occur via passive transport through an ion channel down an electroosmotic gradient, facilitated transport through a co-transporter, or by active transport through ion pumps. For ion channels, the directionality and driving force include both the chemical and electrical components and are defined by Goldman's constant field equation (see Eqs. S4–9) [36]. In the case of transporters and ionic pumps, the molar flux is calculated as a series of Hill terms that modify maximal solute fluxes with predetermined stoichiometry and directionality based on relevant ionic concentrations in the source compartment at any given time (see Eqs. S10, 11) [22, 23]. Through model-estimated permeabilities (ion channels) and maximal fluxes (co-transporters), these terms are used to describe the dynamics for each individual transport pathway. For a more detailed description of the expressions used to describe individual ion channels and transporters, see the Online Resource.

In the paracellular space, we include the transport of solutes through both diffusive and convective means. It is important to note that the model applies the same paracellular transport mechanisms to both ionic and uncharged solutes. With this in mind, we can describe the diffusive $\left(J_{diff}\right)$ and convective $\left(J_{conv}\right)$ components of paracellular solute transport as follows:

$$J_{diff} = P^k_{Ap,Bl} \Delta [k]_{Ap,Bl} \tag{4}$$

$$J_{conv} = [k]_i \frac{dV_{Ap \leftrightarrow Bl}}{dt} \tag{5}$$

Here, $P^k_{Ap,Bl}$ represents the paracellular permeability of solute k, $\Delta [k]_{Ap,Bl}$ and $\frac{dV_{Ap \leftrightarrow Bl}}{dt}$ are the concentration gradient of solute k and the water flux between the Ap and Bl compartments, respectively, as determined by the orientation of the osmotic pressure, $\Delta \pi_{Ap,Bl}$. From these expressions, we can describe a closed system mass balance for any solute, k_i, throughout the three compartments as:

$$\frac{dk_{Ap}}{dt} = -\sum_{Y}^{C,Ap} J_y + J_{diff} + J_{conv} \tag{6}$$

$$\frac{dk_C}{dt} = \sum_{Y}^{C,Ap} J_y + \sum_{Y}^{C,Bl} J_y + \sum_{L} n_k J_{act,l} \tag{7}$$

$$\frac{dk_{Bl}}{dt} = -\sum_{Y}^{C,Bl} J_y - \sum_{L} n_k J_{act,l} - J_{diff} - J_{conv} \tag{8}$$

Here, $\frac{dk_i}{dt}$ is the change of solute k in compartment i, $\sum_Y^{C,i} J_y$ is the summation of all the ion channel (Y) fluxes between the C and either the Ap or Bl compartments, and $\sum_L n_k J_{act,l}$ is the summation of any co-transporter (L) flux multiplied by their respective stoichiometric coefficient, n_k. Notice that this last term is only present between the C and Bl compartments due to the lack of significant facilitated or active ion transport between the Ap and C compartments in airway epithelial cells [9].

Individual ionic currents, I_Y, are calculated for all electrogenic ionic fluxes, J_Y, such that the relation between ion flux and current can be described as:

$$I_Y = \mathrm{F} z_k J_Y \tag{9}$$

where z_k is the ionic charge of solute k, and F refers to Faraday's constant. These currents are used to derive dynamic expressions for the membrane potential across both membranes, such that:

$$\frac{dE_{Ap}}{dt} = C^{-1}_{Ap} A_{ap} \left(-\sum_{Y}^{Ap} I_y + \sum_{k}^{P} I_k \right) \tag{10}$$

$$\frac{dE_{Bl}}{dt} = -C^{-1}_{Bl} A_{Bl} \left(\sum_{Y}^{Bl} I_y + \sum_{k}^{P} I_k \right) \tag{11}$$

were E_i and C_i are the either the apical or basolateral membrane potentials and capacitances per area, respectively. Membrane capacitances are considered constants for both membranes, and are based on previously reported values [37]. For a full description of the model equations, please see Eqs. S1–S44 in Online Resource.

Parameter estimation

Model training and estimation of the 15 free parameters in the model were carried out via our affine-invariant ensemble of samplers with parallel tempering Markov Chain Monte Carlo (APT-MCMC) algorithm, a C++-implemented, Python-wrapped parameter optimization tool for systems of ODEs [38]. APT-MCMC is open-source and publicly available online (https://gitlab.com/liangzha/APT-MCMC). APT-MCMC estimates parameter values by leveraging the dynamic nature of MCMC algorithms to sample a user-defined parametric hyperspace. The algorithm deploys distinct, yet parallelly executed, chains of samplers that explore different temperatures or levels of the model's objective space. The samplers are implemented to

efficiently search regions of highly correlated parametric distributions, a common occurrence in biologically-inspired mathematical models [39]. Each level is defined with varying thermodynamic energies, and permits the inter-chain exchange of information regarding goodness of fit, thus providing information about the breadth and depth of the objective space [40, 41]. APT-MCMC has been successfully implemented for optimization of a clinically-relevant mathematical model of coagulopathies in trauma patients [42].

The model parameters were estimated at the population level in order to generated parametric descriptions of Non-CF and CF HNE cultures. A pooled, logarithmically-transformed sum-of-squared errors objective function (χ^2) was defined between simulation predictions and ASL volume (fitted in mL) and DTPA absorption data (fitted as retention in hundreds of thousands of counts to scale it suitably versus ASL volume). χ^2 computes the cumulative squared deviation of the model simulation against the experimental data from all individual cell cultures from each subject corresponding to a respective cell type, such that:

$$\chi^2(\theta) = \sum_{x=1}^{n}\sum_{k=1}^{m}\sum_{i=1}^{d}\left(\log X^*_{x,k,i} - \log X_x(\theta, t_i)\right)^2 \quad (12)$$

Here, $X^*_{x,k,i}$ refers to the data point recorded for the observable states (ASL or Tc-DTPA) x, for each individual filter for donor k, measured at time point t_i. $X_x(\theta, t_i)$ is the corresponding model-simulated value of each state as predicted by a given parameter set, θ. The objective function was optimized according to:

$$\begin{aligned} \widehat{\theta} &= argmin[\chi^2(\theta)] \\ s.t. X_x &= f(X, \theta, t, X_0) \quad and\ \theta_{min} \le \theta \le \theta_{max} \end{aligned} \quad (13)$$

where $\widehat{\theta}$ represents the parameter values that correspond to the identified solution to the optimization problem, f is the user-defined ODE system, θ is the set of free parameters, X and X_0 are the states and their respective initial conditions, and θ_{min} and θ_{max} are the set of lower and upper bounds for all free parameters. APT-MCMC was used to generate a library of parameter sets that best describe the ASL and Tc-DTPA dynamics of CF and Non-CF HNE cultures, as a function of Eq. 13. Recognizing the multi-dimensionality of the parameter space, special care was taken to guarantee the optimization scheme converge prior to the acceptance of any parameter set. As such, only the top 100 parameter sets for each group were chosen. A list of all free parameters used in the model, and their respective parametric ranges, can be found in Table 2.

Since the model is trained with a dataset that primarily informs paracellular fluxes and transcellular water transport, and in an effort to limit exploration within a biologically-meaningful parametric region, parameter ranges for ion channels and transporters were estimated from a previously published model of airway epithelial electrophysiology under flooded conditions for both non-CF and CF cell cultures [26]. Constant values for cellular volume regulation, electrolyte-transporter affinities, and other airway epithelial physiology descriptors were obtained from literature and previously published models of human airway electrophysiology [23–25, 28, 43–46]. For more details see Table S2.

Results

In vitro ASL and Tc-DTPA transport across healthy and CF HNEs

10 µL of IR solution and DTPA were added to the apical side of non-CF and CF HNE cell cultures as described in the "Materials and methods" section and shown in Fig. 1a. Data demonstrated that CF cultures had decreased ASL

Table 1 HNE donor information and summary measurements

ID	Group size	Age	Sex	Genotype	Isotonic ringers		Hypertonic ringers	
					ASL (% ± SEM)	Tc-DTPA (% ± SEM)	ASL (% ± SEM)	Tc-DTPA (% ± SEM)
CF	9	38 (± 7.4)	M (8)	ΔF508/ΔF508 (4) ΔF508/other (8) Other/other (2)	N = 7 83.2 ± 0.09	61.2 ± 8.3	N = 5 − 23.4 ± 10.9	34.4 ± 6.3
Non-CF	14	28 (± 0.4)	M (9)	wt/wt	N = 12 64.2 ± 0.06	37.5 ± 8.1	N = 6 − 110.2 ± 15.2	36.5 ± 2.9

This includes in vitro ASL and Tc- DTPA clearances from healthy donors (wt/wt) and patients with CF (non-wt/non-wt) following isotonic and hypertonic stimuli. Experimental measurements are reported as the percent (%) change over 24 h (positive: net liquid absorption, negative: net liquid secretion). Means (± SEM) were calculated from all individual cell cultures from each group

Table 2 Model parameters were estimated using APT-MCMC, using a pooled, log-space, and nonlinear least-squares objective function for each population, as described in "Materials and methods" section

Parameter	Units	Non-CF	CF	Parameter axis	Definition
Pwca*	μm/min	1.41×10^4 (731.3)	3.33×10^4 (3.95×10^3)	10,200–18,000	Water permeability, trans-apical
Pwcb*	μm/min	1.31×10^4 (834.4)	3.46×10^4 (6.02×10^3)	8000–18,000	Water permeability, trans-basolateral
Pwab	μm/min	0.97×10^5 (3.25×10^3)	1.0×10^5 (4.22×10^3)	72,000–120,000	Water permeability, paracellular
Penac*	μm/min	2.303 (0.817)	3.359 (0.689)	0.6–6	ENaC permeability
Pcftr	μm/min	2.290 (0.706)	–	0.6–6	CFTR permeability
Pacc*	μm/min	2.584 (0.3603)	0.759 (0.587)	0.6–6	ACC permeability
Pbkca	μm/min	0.862 (0.5870)	0.962 (0.608)	0.6–6	BKCa permeability
Pbk	μm/min	4.094 (0.2045)	3.312 (0.443)	0.6–6	bK permeability
Pbcl	μm/min	3.597 (0.1349)	2.821 (0.564)	0.6–6	bCl permeability
Ppna	μm/min	2.909 (0.466)	3.199 (0.3242)	0.6–6	Na^+ permeability, paracellular
Ppcl	μm/min	2.597 (0.559)	2.566 (0.540)	0.6–6	Cl^- permeability, paracellular
Ppk	μm/min	3.151 (0.334)	3.037 (0.520)	0.6–6	K^+ permeability, paracellular
Ppdt*	μm/min	7.850 (0.559)	8.485 (0.369)	6–10	DTPA permeability, paracellular
Jnkcc	mmol/min m^2	33.51 (5.43)	32.83 (5.77)	6–60	Maximum molar flux through NKCC
Jnakp	mmol/min m^2	29.84 (7.01)	30.44 (7.12)	6–60	Maximum molar flux through Na–K–ATPase

Model includes 15 free parameters describing ion and water permeabilities through both transcellular and paracellular pathways. The permeability of CFTR was assumed to be negligible in the CF case. The Non-CF and CF columns shows the best parameter values obtain (as well as the standard deviation for each parameter calculated from the top 100 parameter sets) for each group, respectively. Parametric axis describes the initial ranges used for the estimation of ion channels and transporter permeabilities. *$p < 0.05$ comparing CF to non-CF by Kolmogorov–Smirnov test ($p < 0.05$). Some of these ranges were based on a previously published model of airway electrophysiology under Ussing Chamber conditions [26]. Full distributions for each parameter are shown in Fig. S1

volumes (μL) at the start of the experiment (t = 0 h) relative to non-CF cultures (10.01 ± 1.38 vs. 15.35 ± 0.95, respectively; p = 0.0019 by student *t* test), indicative of the characteristic dehydration of CF ASL (Fig. 1a). CF samples also showed a significantly depressed ASL volume 24 h after the initial volumetric challenge (1.68 ± 0.38 vs. 5.49 ± 0.90, respectively; p = 0.0027). Percent Tc-DTPA absorption over 24 h was significantly increased in the CF case relative to non-CF (55.40 ± 3.66 vs. 33.51 ± 3.41, respectively; $p = 7.16 \times 10^{-4}$), as shown in Fig. 3b. Previous studies have demonstrated increased rates of DTPA absorption in primary CF HBE cell cultures and in the lungs of CF patients [3, 6, 27]. Previous studies have also shown that there is a strong correlation between ASL volume and Tc-DTPA absorption in non-CF HBE cultures [6]. In an effort to further corroborate these observations in HNE, total ASL and Tc-DTPA absorption were calculated from each subject-specific set of cultures and correlated (Pearsons's *r*), see Fig. 3c. The analysis confirmed that for non-CF cell cultures, ASL volume and Tc-DTPA

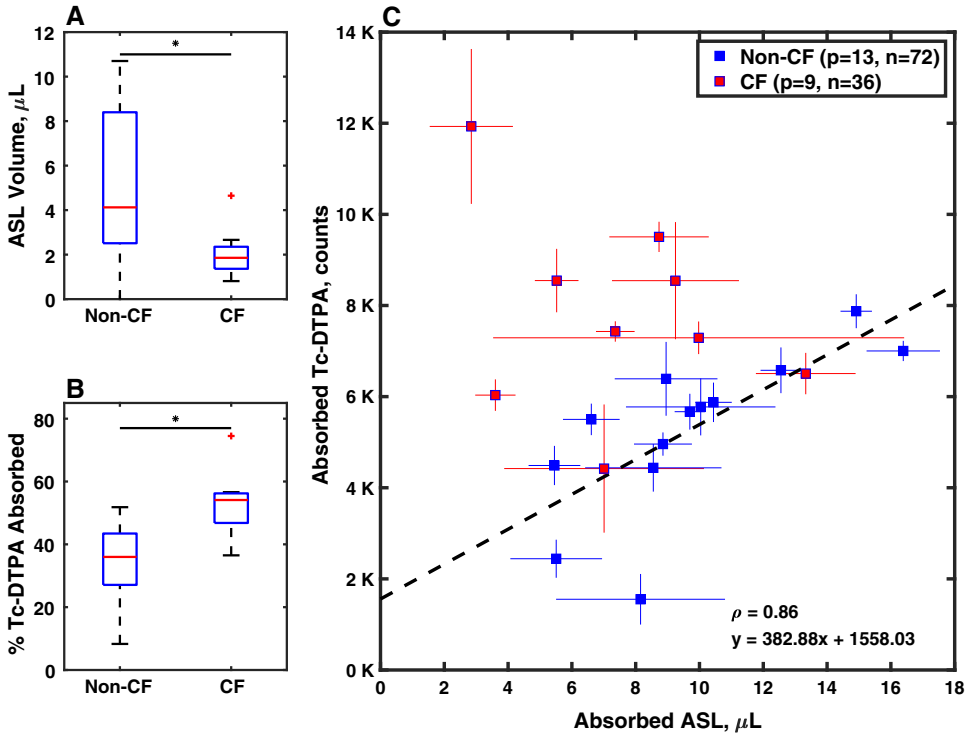

Fig. 3 Summary of ASL and Tc-DTPA absorption profiles for non-CF and CF HNE cell cultures. **a** Final ASL volume 24 h following the addition of 10 μL of isotonic Ringer's solution and Tc-DTPA. CF cultures demonstrated a significantly decreased final ASL volume relative to non-CF cell cultures (p = 0.0209). **b** Percent Tc-DTPA absorbed.CF cell cultures had higher Tc-DTPA absorption rates than non-CF cultures ($p = 9.708x10^{-4}$). **c** Comparison plot showing the relationship between Tc-DTPA absorbed (thousands of counts) and ASL volume absorbed (μL) for both non-CF (13 patients, 72 filters, blue squares) and CF (9 patients, 36 filters, red squares) 24 h after the initial volumetric challenge. The dashed line represents the linear regression for non-CF cultures which shows strong correlation between the measurements ($\rho = 0.86$). CF cultures show a significant upwards deflection relative to the fitted line, suggesting an increased rate of Tc-DTPA absorption independent of liquid movement (diffusive component). Comparisons by unpaired t-test. Statistical significance is indicated as * (Color figure online)

absorption are strongly correlated ($\rho = 0.86$). A similar analysis for CF cell cultures showed the breakdown of this relationship due to increased Tc-DTPA clearance.

Transcellular water transport as a driver of cystic fibrosis pathophysiology

Model simulations were able to capture the absorption dynamics of the ASL and Tc-DTPA, for both CF and non-CF cell cultures, using an identical structure, as shown in Fig. 4. The model-predicted apical volume and Tc-DTPA trajectories were within the standard error of the mean for all time points in both cases. Population-level parameter distributions were generated for all free parameters listed in Table 2, according to the procedure described in the *Parameter Estimation* subsection. Comparisons between the model-predicted distributions of CF and non-CF cultures were performed using a 2-sample, unpaired Kolmogorov–Smirnov (2-KS) test. The model predicts that CF cultures, relative to non-CF cultures, have increased apical (P_{wac}: 3.33×10^4 vs. 1.41×10^4, respectively; $p = 4.329 \times 10^{-9}$) and basolateral (P_{wcb}: 3.46×10^4 vs. 1.31×10^4, respectively; $p = 7.583 \times 10^{-8}$) water permeabilities (Fig. 5a, b). On the other hand, paracellular water permeability was similar in CF and non-CF cultures (P_{wab}: 1.02×10^5 vs. 0.97×10^5; p = 0.936) (Fig. 5c). These results suggest that transcellular water transport, and not paracellular, is responsible for the hyperabsorptive phenotype observed in CF cell cultures.

Furthermore, the model predicted a statistically significant increase in the paracellular Tc-DTPA permeability for the CF relative to non-CF groups (P_{pdt}: 8.48 vs. 7.85, respectively; p = 0.0376; Fig. 5d). The model also estimated that CF cultures exhibit significantly increased ENaC permeability, P_{ENaC}, and decreased constitutively active (i.e. not CFTR) chloride channel permeability, P_{ACC}, which correlates to observations from the literature (Fig. S1) [25, 47].

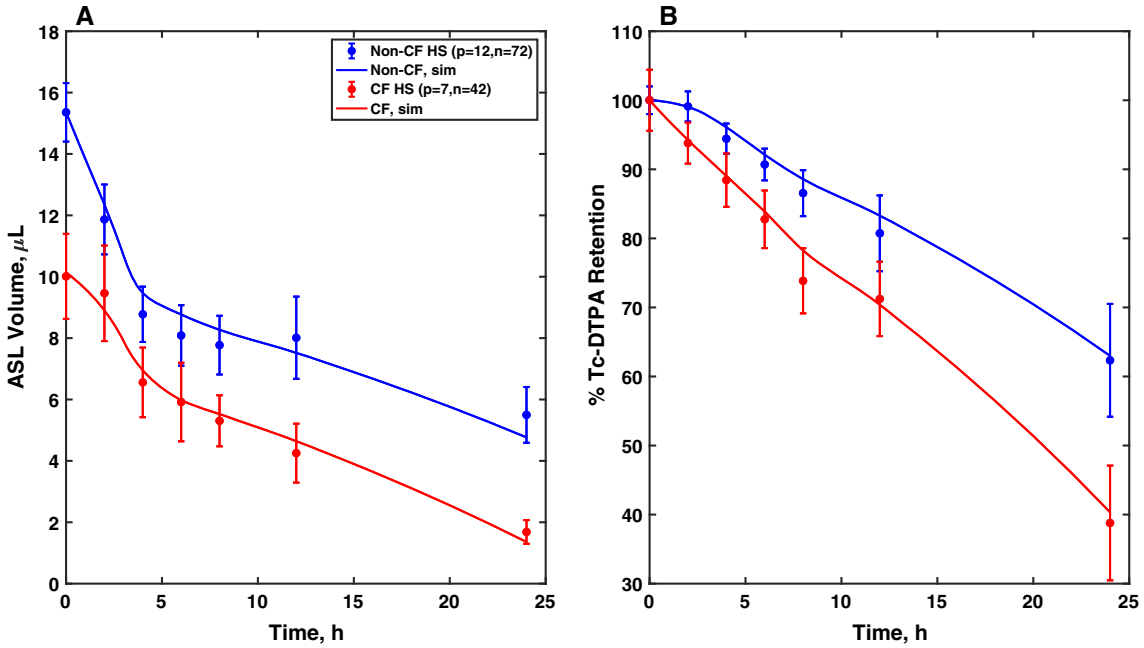

Fig. 4 Best-fit model trajectories (solid lines) and experimental data (error bars; population mean ± SEM) from HNE cell cultures following the apical addition of 10 μL of Isotonic Ringers with Tc-DTPA to 12 non-CF (72 filters) and 7 CF (42 filters) lines. **a** CF lines have lower ASL volumes than non-CF lines at the start and end of the experiment ($p < 1 \times 10^{-4}$). Total predicted volume absorbed is 9.85 ± 0.934 μL (64.2%) in the non-CF lines and 8.33 ± 0.886 μL (83.2%) in the CF lines. Non-CF cells rapidly return to homeostatic ASL volumes (t = 4–12 h), whereas CF cells exhibit a more prolonged absorption profile. **b** CF cultures displayed consistently higher Tc-DTPA absorption rates ($p < 1 \times 10^{-4}$) versus non-CF. Model-estimated DTPA clearance is 37.7% in non-CF cells compared to 61.2% in CF after 24 h

Comparison of DTPA convection and diffusion

Since Tc-DTPA can only move through the paracellular space, the equation describing apical Tc-DTPA counts ($DTPA_{Ap}$), contains no active or passive flux terms into or out of the cell. Thus, the transport equation reduces to:

$$\begin{aligned}\frac{dDTPA_{Ap}}{dt} &= J_{diff} + J_{conv} \\ &= -P_{DTPA_{A,B}}\left(\frac{DTPA_{Ap}}{V_A} - \frac{DTPA_{Bl}}{V_B}\right) \\ &\quad + \frac{DTPA_{Ap}}{V_A}\left(\frac{dV_A}{dt}\right)\end{aligned} \tag{14}$$

The equation for basolateral Tc-DTPA counts ($DTPA_{Bl}$) has opposite directionality but equal structure to Eq. 13, as the two are linked by a mass balance. Each flux term on the right-hand side of Eq. 13 was integrated individually for the 100 best parameter sets obtained after fitting. The cumulative percent Tc-DTPA absorbed via diffusion was calculated at every experimentally-measured time point for both CF and non-CF cultures. The model predicts that over a period of 24 h, CF cultures on average clear 61.9% Tc-DTPA through diffusion, a significantly higher amount when compared to non-CF cultures (49.7%, $p = 1.034 \times 10^{-4}$; see Fig. 6). It should be noted that the percent of Tc-DTPA clearance due to convection will simply be the complementary fraction. Thus, the ~ 40% DTPA absorption estimated as due to convection in CF HNE is similar to experimental values previously reported in CF HBE [10].

Experimental validation

In order to test the model's ability to capture different experimental conditions, the model was used to simulate the results from a test data set. The test data set consisted of non-CF (6 subjects, 22 filters) and CF (5 subjects, 22 filters) ASL and Tc-DTPA retention curves over a period of 24 h following the treatment with HR solution. The increased osmolarity of HR solution, relative to IR, is due to NaCl. Based on its high NaCl proportion, HR may be thought of as a surrogate for hypertonic saline which is a common inhaled osmotic therapy given to CF patients [48]. The addition of HR to both CF and non-CF HNE reverses liquid hyperabsorption, inducing apical volume swelling and arresting paracellular convection of Tc-DTPA. Paracellular diffusion of Tc-DTPA does continue under these circumstances. In the non-CF case, liquid secretion resulted in an initial ASL increase and peak volume was reached approximately 2 h into the experiment after which ASL volume began to be absorbed, possibly re-introducing paracellular convection (Fig. 7). However, the relatively

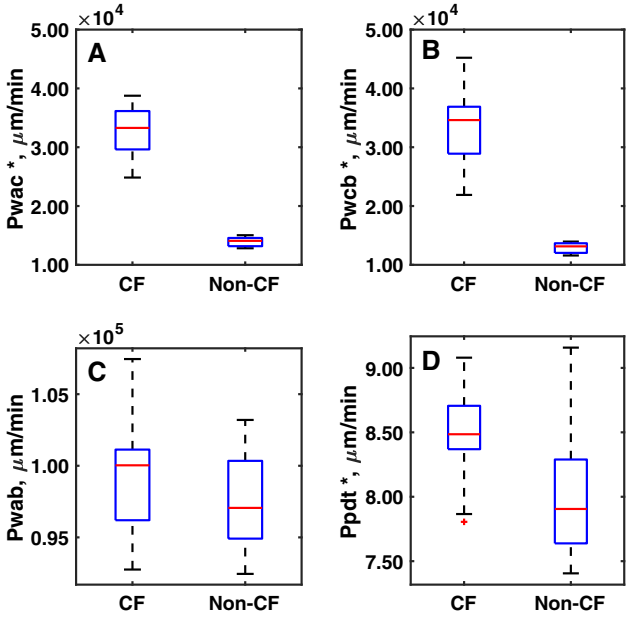

Fig. 5 Comparison plot of the model-predicted distributions of water permeability (**a** apical, **b** basolateral, **c** paracellular) and DTPA permeability **d** for both CF and non-CF cell cultures. *Significant differences between CF and non-CF distributions by a 2-sample Kolmogorov–Smirnov test. Model predicts that both the apical and basolateral water permeabilities (P_{wac} and P_{wcb}, respectively) are increased in CF cultures versus non-CF cultures ($p = 4.329 \times 10^{-9}$ and $p = 7.583 \times 10^{-8}$). However, paracellular water permeability is similar between the two population ($p = 0.936$). Tc-DTPA permeability is increased in CF ($p = 0.0376$). All distributions were generated by pooling the top 100 parameter sets obtain from the parameter estimation scheme for each group, as describe in the Methods

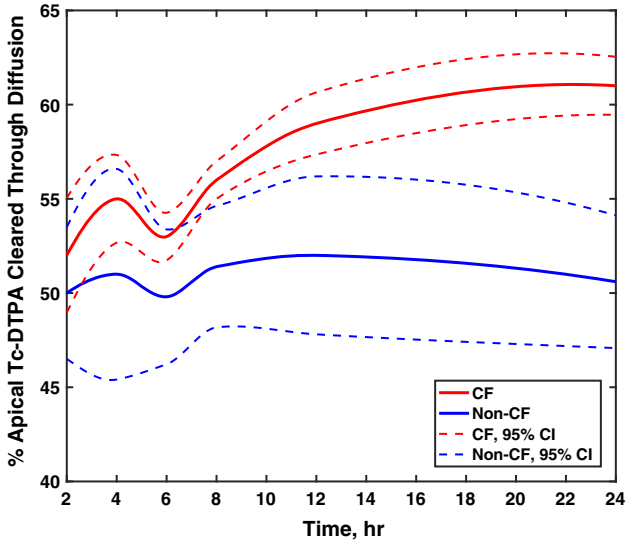

Fig. 6 Model-predicted percent of Tc- DTPA cleared through diffusion for CF and non-CF HNE cell cultures following the apical addition of 10 μL of isotonic Ringer's solutions and Tc-DTPA (diffusion + convection = 100%). Model predicts CF cultures (red) on average clear 61.9% Tc-DTPA through diffusion, a significantly higher amount when compared to non-CF cultures (blue, 51.7%, by student t-test $p = 1.034 \times 10^{-4}$) over a period of 24 h. Solid lines are the mean percent and dashed lines are the 95% confidence intervals. Both measures are calculated from simulations generated from the top 100 parameter sets (based on goodness of fit) (Color figure online)

stable apical Tc-DTPA retention suggests the majority of water transport occurs transcellularly at this stage (Fig. 7). ASL volume showed minimal changes after 8 h (Fig. 7). This implies the observed Tc-DTPA profiles following 8 h represent a strictly diffusive regime (Fig. 7). In the CF case, HR also induced epithelial fluid secretion. However, the cultures showed a significantly reduced rate of ASL reabsorption, see Fig. 7. Tc-DTPA absorption rates were diminished and remained statistically similar to corresponding rates in the non-CF case for most of the experiments (Fig. 7), further suggesting a change in the diffusive driving force for Tc-DTPA.

Validation simulations were carried out by changing in silico exprimental conditions to match those of the testing data set (initial ASL volume, Tc-DTPA counts and electrolyte concentrations), while keeping parameter sets the same as those estimated from the training data set (IR conditions) for each group. The model demonstrates good agreement between predictions and data, even in the case of ASL volume where transport dynamics are quite different (fluid secretion instead of absorption) relative to the training set. In particular, the model succesfully captures the initial rise of ASL volume followed by a slower correction to steady state for both CF and non-CF cultures, as well as the observed increase of apical Tc-DTPA retention for CF cultures. However, the model under predicts the rate of ASL volume reabsorption immediately following the ASL peak volume, see Fig. 7a. The absence or possible delay of this resorptive behavior suggests a possible shift in water permeability as a function of osmotic stimuli in the non-CF and CF cultures that cannot be described without reparameterization. This type of response to osmotic stimuli has been observed in other types of epithelial tissues under similar conditions and time frames [49, 50].

ASL dehydration drives increased Tc-DTPA transport in CF HNEs

The training data set was used to compare ASL and Tc-DTPA end point behaviors between the IR and HR conditions, thus allowing the verification of model predictions. First, we compared the percent apical Tc-DTPA cleared 24 h after the HR osmotic challenge for both CF and non-CF HNE cultures (Fig. 8a). HR significantly reduced the percent of Tc-DTPA absorption relative to IR in CF cultures ($p = 2.003 \times 10^{-4}$), but HR did not affect Tc-DTPA retention in the non-CF ($p = 0.934$) cultures. Since the bulk of convective flux is stopped under these conditions, we

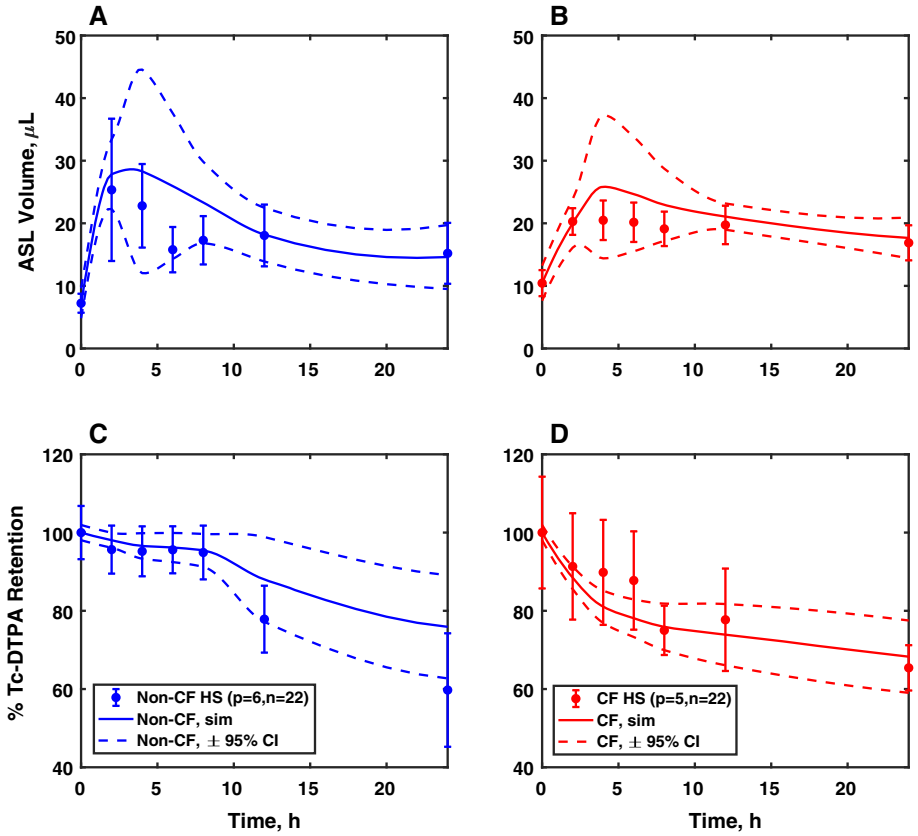

Fig. 7 Model predictions demonstrate good agreement with experimental data from a validation data set. Testing data was from non-CF (6 patients, 22 filters, blue squares) and CF (5 patients, 22 filters, red squares) cultures and included ASL and Tc-DTPA retention curves following the treatment with HR solution. Validation simulations were carried out by changing in silico exprimental conditions (initial ASL volume, apical electrolyte/Tc-DTPA concentrations (HR = IR + 200 mM NaCl)) to match those of the testing dataset, and using the top 100 parameter sets for CF and non-CF groups estimated from the training data set (IR conditions). There is good agreement between model prediction and data, eventhough transport dynamics are quite different from the training conditions (fluid secretion instead of absorption). In particular, the model succesfully captures the initial rise of ASL volume with HR followed by a slower correction to steady state for both CF and non-CF cultures and an observed increased of apical Tc-DTPA retention for CF cultures, relative to the training data set (IR, Fig. 3). Solid lines represent the best parametric fit for each group. Dashed lines are the 95% confidence intervals calculated from model-predicted values for each parameter set included in the distributions shown in Figs. 6, and S1 (Color figure online)

explored changes in the diffusive driving force. In Fig. 8b, we calculated the fold change in apical Tc-DTPA concentration as a function of time for HR studies relative to the IR studies. In the CF cultures, apical concentration of Tc-DTPA was significantly reduced with HR relative to IR, much more so than for non-CF cultures (maximum fold change: $\sim$ 7 vs. $\sim$ 3, CF vs non-CF; p = 1.092×10^{-4}). This reveals that the observed hyperabsorption of Tc-DTPA in CF cultures (Fig. 3a) is likely due to depressed apical volume, leading to a consistently higher diffusive driving force relative to non-CF cultures. Lastly, total change in ASL volume and Tc-DTPA absorption were calculated from each donor in the testing data set (HR conditions) and tested for correlation (Fig. 8c). The analysis revealed the loss of the strong correlation previously observed for non-CF cultures under IR conditions $((r = 0.09)$ vs. $(r = 0.86)$ (Fig. 3c), p = 0.83). Since the cornerstone of this relationship is the now osmotically depressed convective Tc-DTPA transport, its absence further confirms the amplyfing effect that ASL dehydration has on diffusive Tc-DTPA transport in CF cells.

Discussion

The model presented herein accurately captures ASL and Tc-DTPA dynamics within biologically-meaningful parametric ranges allowing for a mechanistic exploration of the physiological differences between CF and non-CF epithelia. The trajectories also highlight differences in absorption kinetics between the non-CF and CF cultures. Non-CF cells rapidly reabsorbed liquid and return to homeostasis while

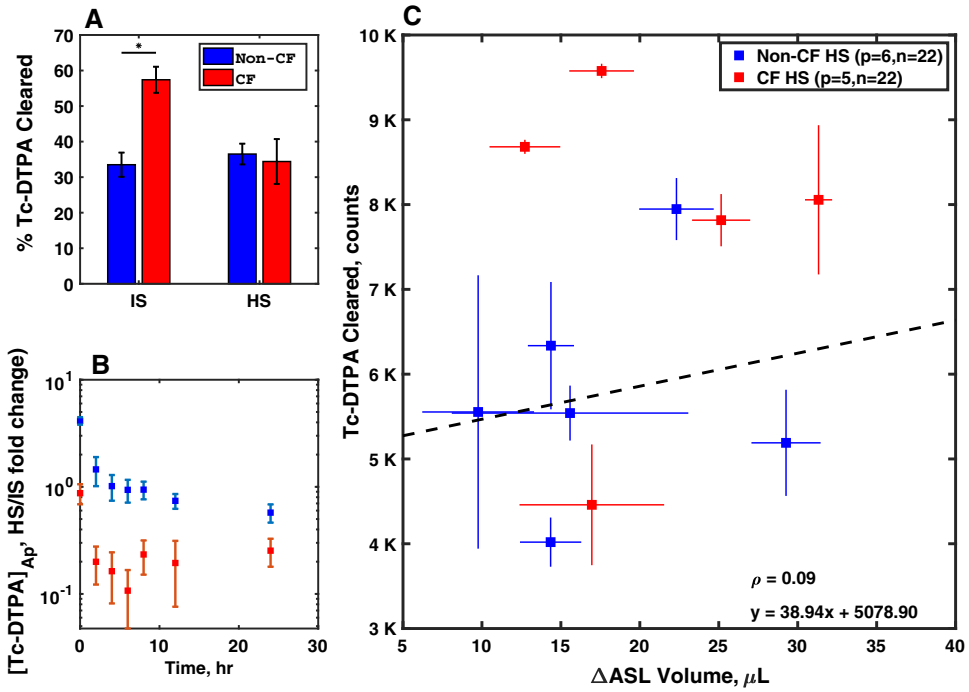

Fig. 8 Summary of ASL and Tc-DTPA clearance for non-CF and CF HNE cell cultures following the apical addition of 10 μL of Hypertonic Ringer's solutions (isotonic + 200 NaCl mM) and Tc-DTPA. **a** Percent apical Tc-DTPA cleared 24 h after the HR osmotic challenge for both CF and non-CF HNE cultures. It shows that HR significantly reduces the percent of Tc-DTPA absorbed relative to IR in CF ($p = 2.003 \times 10^{-4}$), but not in non-CF ($p = 0.934$) cultures. Comparisons by unpaired t-test,*$p < 0.05$. **b** Apical Tc-DTPA concentration as a function of time calculated as the fold change with HR relative to the IR. This reveals that the observed hyperabsorption of Tc-DTPA in CF cultures is likely due depressed apical volume, leading to a consistently higher driving force relative to non-CF cultures ($p = 1.092 \times 10^{-4}$). **c** Comparison plot showing the relationship between Tc-DTPA absorbed (thousands of counts) and ASL volume absorbed (μL) for both non-CF (6 patients, 22 filters, blue squares) and CF (5 patients, 22 filters, red squares) 24 h after the initial osmotic and volumetric challenge. The dashed line represents the linear regression for non-CF cultures. The relationship between ASL and DTPA absorption previously demonstrated with IR (Fig. 3) is not apparent after HR addition ($r = 0.09$) (Color figure online)

CF cells demonstrated a slower rate, but longer duration, of liquid absorption that ultimately leads to a decreased standing apical volume. In addition to good dynamic agreement between model output and experimental data, the parameters agreed well with those found in literature. The total epithelium water permeabilities in both the CF and non-CF cases were similar to those reported by Matsui and colleagues [46].

Because ion transport defects and airway surface liquid dehydration both play key roles in CF lung disease, it is important be able to characterize liquid and solute transport. Our model demonstrates that the main factor contributing to differences in absorption dynamics between CF and non-CF epithelia are transcellular hydraulic permeabilities (Fig. 5a, b, Table 2), which it predicts as being nearly threefold higher in CF. The model-predicted paracellular hydraulic permeabilities were not significantly increased in CF (Fig. 5c). This suggests that transcellular permeability has a larger role in the observed decreased ASL volume in CF than paracellular permeability. Our model also corroborates previous reports, both in vitro [6] and in vivo [5], that radiolabeled DTPA conjugates' absorption is increased in the CF airway. While ASL can be transported through trans- or paracellular pathways, Tc-DTPA can only be cleared paracellularly, either through diffusive or convective transport. Since the convective component of Tc-DTPA absorption is directly driven by ASL absorption, the relationship between Tc-DTPA and ASL absorption can be used to illustrate the relative contributions of convection and diffusion. For example, the increased Tc-DTPA absorption observed in Fig. 3c for CF cultures, relative to the non-CF trendline, suggests a Tc-DTPA absorption rate increase that is independent of liquid movement (i.e. through diffusion). Using our mathematical description of Tc-DTPA absorption from the ASL, we are able to probe the relative contributions of diffusion and convection that lead to increased solute absorption in CF. The model predicts that diffusive transport accounts for approximately 60% of all Tc-DTPA absorption seen in CF, a significant increase relative to the 49% predicted for non-CF cells, which is close to experimentally observed values [10]. It is likely that diffusion transport rates are increased in CF due to the decreased initial ASL volume and identical added Tc-DTPA counts in both CF and non-CF

experiments. Thus, the concentration, and therefore the diffusive driving force, was slightly increased in CF over the course of the experiments.

Additionally, the model-determined ion channel permeabilities were within parametric ranges previously published in a model of HBE under Ussing Chamber conditions [26]. These model-predicted parameters also corroborate previous results describing the function of epithelial ion channels. For instance, the model estimated that ENaC permeability is significantly increased in CF cell cultures (Fig. S1), which is in agreement with the findings of previous experimental and modeling studies [25, 47]. Furthermore, the model predicted a significant increase in the constitutively active (i.e. not CFTR) chloride channel permeability in our model, P_{ACC}, in non-CF cell cultures (Fig. S1). These results are in line with the findings of Bertrand et al., who have reported that SLC26A9, a constitutively active Cl^- channel expressed in the apical membrane of airway epithelia, shows diminished expression and functional levels in the presence of dysfunctional CFTR [14, 51]. Overall, our model describes hyperabsorptive liquid and solute dynamics in CF that are associated with a loss of CFTR function and the subsequent loss of ENaC flux and decreased constitutive Cl^- transport.

Previous mathematical models of airway epithelia have considered liquid and solute transport in varying degrees of mechanistic detail. The majority of these models have been designed for non-physiological conditions where the extracellular compartment volumes are static. A more recent model includes dynamic apical and basolateral compartments and thin film conditions [28]. These conditions recreate the conditions in the human airway, allowing the modeled epithelium to establish a homeostatic ASL at an air–liquid interface. Our model further accounts for paracellular transport and includes dynamic apical, basolateral, and cellular compartments under thin-film conditions. Airway epithelia are also known to transport solutes beyond Na^+, Cl^-, and K^+ that can play a role in the regulation of ion and liquid transport (e.g., Nucleotides, HCO_3^-, H^+, Ca^{2+}). However, in an effort to minimize parameter uncertainty and complexity, these were not included herein as explicit model states. Instead, the model is focused on further developing the description of paracellular solute transport. It is recognized that purinergic, pH and Ca^{2+} fluctuations can have meaningful effects on the function of several ion channels, transporters, and consequently, transepithelial water transport and possibly even MCC [52–55]. However, previously published work also suggests that under baseline conditions (i.e. in the absence of a purinergic/mechanical stimuli) the homeostatic levels of nucleotides and nucleosides are largely unchanged, even in the presence of large ASL volume differences [54]. As a result, we postulate that these signaling dynamics do not play a significant role under conditions that do not explicitly induce a change in their respective baseline values. As such, they were not explicitly included in the model structure. Rather, our model considers the effects that ASL and cell volume have on regulating solute and liquid flux in an HNE culture system. It is quite possible that both mechanisms (purinergic and volumetric) are related, or a consequence of one another. However, the volumetric effect modeled herein captures the available experimental data in a structurally simple manner.

Our model also includes a more descriptive understanding of paracellular ion fluxes. Current literature describes paracellular ionic transport using Goldman's constant field equation, the same expression used for transcellular ion channel fluxes [24, 28]. This approximation fails to account for the contributions of diffusive transport along the entire paracellular pathway and convective transport due to fluid drag. Previous work from our group has shown that convective transport can account for approximately 50% of Tc-DTPA transport across primary HBE cell cultures [10]. This suggests convection could also play a significant role in the paracellular transport of ionic species. Specifically, we compared predicted paracellular electrolyte fluxes in the electroosmotic versus the combined convection plus diffusion case. Our results suggest that electrical contributions are effectively negligible after the inclusion of convective driving forces [Na: 9.83×10^{-9} vs. 2.01×10^{-7}; Cl: 8.07×10^{-9} vs. 1.81×10^{-7}; K: 9.59×10^{-10} vs. 5.18×10^{-8}, respectively (mmol/min)]. Detailed calculations can be found in table S3 in the Online Resource. This distinction is particularly important under conditions of non-homeostatic hydraulic flux, such as those following a volumetric or tonicity challenge of the ASL. Our group has previously shown that in HBE cultures, an apical to basolateral osmotic, but not chemical, equilibrium abolished approximately 50% of Tc-DTPA transport in CF HBEs [10]. Furthermore, while electroosmotic transport is likely representative of charged solute transport across the tight junction, it does not account for the effects that the inherent paracellular pathway tortuosity and length of an epithelial membrane are likely to have on the effective solute permeabilities of larger, uncharged molecules such as Tc-DTPA, or the charge selectivity function that some tight junction proteins may exert on ionic solutes [56]. A detailed understanding of the dynamic nature of these effects is a largely underexplored area and could warrant further study.

We validated the model using 6 non-CF and 5 CF cultures from the cell lines included in the training set but exposed to different experimental conditions. Validation testing was performed by measuring ASL and Tc-DTPA

response following the addition of 10 μL of HR with Tc-DTPA to the ASL. Model simulations were carried out using line-specific parameter data obtained during training (IR) experiments. Only initial apical volumes, Tc-DTPA counts, and ionic concentrations were changed to reflect experimental conditions. Model prediction of experimental results was acceptable in both the CF and non-CF cases overall. The model was able to capture the maximum observed ASL volume increase following the osmotic challenge, and the final steady state (Fig. 7a). However, the model struggled to recapitulate reabsorption dynamics for non-CF cultures in particular. This may suggest a possible shift in the expression or functional regulation profile of aquaporins as a result of the hyperosmotic challenge. This type of behavior has been observed in epithelial tissues in both the gut and urinary tract [49, 50]. HR reduced the percent of Tc-DTPA absorbed in CF cultures to levels comparable to those of non-CF cultures under IR conditions. A similar shift, however, was not observed in non-CF cultures (Fig. 8a). Since ASL absorption was largely abrogated with HR, Tc-DTPA absorption under these conditions is likely caused by diffusion. This is supported by the loss of the correlation between ASL and Tc-DTPA absorption following HR treatment, which is driven by the convective transport (Fig. 8c). Further investigation revealed that the reduction in Tc-DTPA absorption observed in CF cultures following HR treatment was primarily driven by changes in apical Tc-DTPA concentration. Because of their increased transcellular water transport, CF cultures experience a higher degree of apical solute dilution ($\sim$ sevenfold change) than non-CF cultures ($\sim$ twofold change) under HR conditions relative to IR ones (Fig. 8b). The dilution of apical Tc-DTPA leads to a corresponding reduction of chemical driving force. This loss, alongside the higher Tc-DTPA permeability predicted by the model (Fig. 5d), results in an abrogated Tc-DTPA diffusive transport rates in CF under hypertonic conditions. This finding is particularly important, because it provides a better mechanistic understanding of radiolabeled DTPA absorption as a biomarker of CF liquid hyperabsorptive phenotype both in vitro and in vivo.

HR acts as a direct in vitro surrogate for hypertonic saline (HS) [10]. Inhaled HS is a vital therapy for patients with CF, and its prescribed to approximately 72% of CF patients age 6 or older [57]. Because of its tonicity, when inhaled, HS acts as a mucus thinning agent that temporarily rescues the airway hyperabsorption phenotype, promoting MCC [48, 58–60]. Chronic treatment with inhaled HS has also been linked with higher lung function and reduced rate of pulmonary exacerbation among CF patients [61]. More recently, the FDA has approved the use of inhaled powder mannitol as an alternative osmotic therapy to HS in the treatment of CF patients [62]. Mannitol has a similar mechanism of action to HS, but since it is only transported paracellularly, its residence time in the ASL, and therefore its effective window, is thought to be prolonged [27, 62–65]. DTPA and mannitol share similar transport mechanisms, as such, DTPA transport studies in the airway both in vitro, as the ones described here, and in vivo are vital in order to understand the dynamics of inhaled osmotic therapeutics such as mannitol. It is worth pointing out, the model described here could also be extended to other inhaled small molecule therapeutics both in CF and other airway pathologies. Specifically, this work could be applied to the optimization of novel dosing strategies for other categories of inhaled therapeutics such a bronchodilators and antibiotics, where ASL retention is preferred over absorption [66, 67].

Ultimately, we envision the development of in silico models that are informed by data relating in vitro cell physiology and therapeutic response to in vivo organ physiology and therapeutic response, and eventually clinical outcomes. These models could be applied to develop personalized therapeutic strategies for CF patients. They could also provide new parameters for phenotyping CF subjects and a better understanding of the physiological effects of CFTR function and specific genotypes. This notion is particularly relevant because our model is able to track the different modes of liquid and Tc-DTPA transport in HNE cultures grown from cells harvested from specific patients. This connection would suggest the in vitro and in silico descriptors of Tc-DTPA dynamics implemented here could correlate with their corresponding In-DTPA absorption (ABS) measurements, a DTPA-based in vivo biomarker of airway absorption. Current studies are underway to characterize nasal cell culture physiology, organ level physiology, and clinical outcomes in cohorts of CF subjects, single CFTR mutation carrier who are parents of CF patients, and healthy controls (NCT02947126), that are intended to inform such models. These studies include nuclear imaging studies to measure mucociliary clearance and ABS in the lungs.

We have previously observed and modeled MCC and DTPA absorption in the lungs of subjects with and without CF [3, 10, 27]. These previous studies provide a quantitative and mechanistic description of ABS, and MCC. Similarly, this work represents a mechanistic description of DTPA and liquid transport that is relevant at a sub-scale of our previous work. Whole-organ model development based on this scan data is ongoing. Ultimately, the multi-scale linkage of in vitro models to the whole-organ model, including patient-specific disease mechanism and clinical performance data, will facilitate the design and use of multi-scale models in patient-tailored and population-scale interventions for CF patients.

Acknowledgements The authors thank Stefanie Coburn and Sheila Frizzell for their technical assistance with cell cultures, and Mary Joens, Matthew Markovetz, Ph.D., and William Confer for contributions to model development and implementation. As well as funding from the National Institutes of Health Grants # R01 HL108929-01 and U01 HL131046-01.

References

1. The Cystic Fibrosis Foundation About Cystic Fibrosis. https://www.cff.org/What-is-CF/Genetics/Types-of-CFTR-Mutations/%0D%0A
2. Orestein David M, Spahr Jonathan E, Weiner DJ (2012) Cystic fibrosis: a guide for patient and family, 4th edn. Lippincott Williams & Wilkins, Philadelphia
3. Locke LW, Myerburg MM, Weiner DJ et al (2016) Pseudomonas infection and mucociliary and absorptive clearance in the cystic fibrosis lung. Eur Respir J 47:1392–1401. https://doi.org/10.1183/13993003.01880-2015
4. Pilewski JM, Frizzell RA (1999) Role of CFTR in airway disease. Physiol Rev 79:S215–S255
5. Corcoran TE, Thomas KM, Myerburg MM et al (2010) Absorptive clearance of DTPA as an aerosol-based biomarker in the cystic fibrosis airway. Eur Respir J 35:781–786. https://doi.org/10.1183/09031936.00059009
6. Corcoran TE, Thomas KM, Brown S et al (2013) Liquid hyperabsorption as a cause of increased DTPA clearance in the cystic fibrosis airway. EJNMMI Res 3:14. https://doi.org/10.1186/2191-219X-3-14
7. Tarran R, Button B, Boucher RC (2006) Regulation of normal and cystic fibrosis airway surface liquid volume by phasic shear stress. Annu Rev Physiol 68:543–561. https://doi.org/10.1146/annurev.physiol.68.072304.112754
8. Verkman AS (1998) Role of aquaporin water channels in kidney and lung. Am J Med Sci 316:310–320. https://doi.org/10.1097/00000441-199811000-00004
9. Hollenhorst MI, Richter K, Fronius M (2011) Ion transport by pulmonary epithelia. J Biomed Biotechnol 2011:174306. https://doi.org/10.1155/2011/174306
10. Locke LW, Myerburg MM, Markovetz MR et al (2014) Quantitative imaging of airway liquid absorption in cystic fibrosis. Eur Respir J 44:675–684. https://doi.org/10.1183/09031936.00220513
11. Vazquez E, Nobles M, Valverde MA (2001) Defective regulatory volume decrease in human cystic fibrosis tracheal cells because of altered regulation of intermediate conductance Ca^2+-dependent potassium channels. Proc Natl Acad Sci USA 98:5329–5334. https://doi.org/10.1073/pnas.091096498
12. Birket SE, Chu KK, Liu L et al (2014) A functional anatomic defect of the cystic fibrosis airway. Am J Respir Crit Care Med 190:421–432. https://doi.org/10.1164/rccm.201404-0670OC
13. Myerburg MM, Harvey PR, Heidrich EM et al (2010) Acute regulation of the epithelial sodium channel in airway epithelia by proteases and trafficking. Am J Respir Cell Mol Biol 43:712–719. https://doi.org/10.1165/rcmb.2009-0348OC
14. Bertrand CA, Mitra S, Mishra SK et al (2017) The CFTR trafficking mutation F508del inhibits the constitutive activity of SLC26A9. Am J Physiol 312:L912–L925. https://doi.org/10.1152/ajplung.00178.2016
15. Kis A, Krick S, Baumlin N, Salathe M (2014) Airway hydration, apical K Secretion, and the large-conductance, Ca-activated and voltage-dependent potassium (BK) channel. Ann Am Thorac Soc 13:163–168. https://doi.org/10.1513/annalsats.201507-405kv
16. Schreiber R, Nitschke R, Greger R, Kunzelmann K (1999) The cystic fibrosis transmembrane conductance regulator activates aquaporin 3 in airway epithelial cells. J Biol Chem 274:11811–11816
17. Jourdain P, Becq F, Lengacher S et al (2014) The human CFTR protein expressed in CHO cells activates aquaporin-3 in a cAMP-dependent pathway: study by digital holographic microscopy. J Cell Sci 127:546–556. https://doi.org/10.1242/jcs.133629
18. Coyne CB, Vanhook MK, Gambling TM et al (2002) Proinflammatory. Cytokines. https://doi.org/10.1091/mbc.e02
19. Molina S, Stauffer B, Moriarty HK et al (2015) Junctional abnormalities in human airway epithelial cells expressing delF508 CFTR. Am J Physiol Lung Cell Mol Physiol. https://doi.org/10.1152/ajplung.00060.2015
20. Van Goor F, Hadida S, Grootenhuis PDJ et al (2009) Rescue of CF airway epithelial cell function in vitro by a CFTR potentiator, VX-770. Proc Natl Acad Sci USA 106:18825–18830. https://doi.org/10.1073/pnas.0904709106
21. Eckford PDW, Ramjeesingh M, Molinski S et al (2014) VX-809 and related corrector compounds exhibit secondary activity stabilizing active F508del-CFTR after its partial rescue to the cell surface. Chem Biol 21:666–678. https://doi.org/10.1016/j.chembiol.2014.02.021
22. Novotny JA, Jakobsson E (1996) Computational studies of ion-water flux coupling in the airway epithelium. II. Role of specific transport mechanisms. Am J Physiol 270:C1764–C1772
23. Falkenberg CV, Jakobsson E (2010) A biophysical model for integration of electrical, osmotic, and pH regulation in the human bronchial epithelium. Biophys J 98:1476–1485. https://doi.org/10.1016/j.bpj.2009.11.045
24. Garcia GJM, Boucher RC, Elston TC (2013) Biophysical model of ion transport across human respiratory epithelia allows quantification of ion permeabilities. Biophys J 104:716–726. https://doi.org/10.1016/j.bpj.2012.12.040
25. O'Donoghue DL, Dua V, Moss GWJ, Vergani P (2013) Increased apical Na^+ permeability in cystic fibrosis is supported by a quantitative model of epithelial ion transport. J Physiol 591:3681–3692. https://doi.org/10.1113/jphysiol.2013.253955
26. Serrano Castillo F, Bertrand CA, Corcoran TE et al (2018) A dynamic model of cystic fibrosis airway epithelium electrophysiology. IFAC-PapersOnLine 51:94–97. https://doi.org/10.1016/j.ifacol.2018.09.027
27. Markovetz MR, Corcoran TE, Locke LW et al (2014) A physiologically-motivated compartment-based model of the effect of inhaled hypertonic saline on mucociliary clearance and liquid transport in cystic fibrosis. PLoS ONE. https://doi.org/10.1371/journal.pone.0111972
28. Sandefur CI, Boucher RC, Elston TC (2017) Mathematical model reveals role of nucleotide signaling in airway surface liquid homeostasis and its dysregulation in cystic fibrosis. Proc Natl Acad Sci USA 114:E7272–E7281. https://doi.org/10.1073/pnas.1617383114
29. Lavelle GM, White MM, Browne N et al (2016) Animal models of cystic fibrosis pathology: phenotypic parallels and divergences. Biomed Res Int. https://doi.org/10.1155/2016/5258727
30. Scholte BJ, Colledge WH, Wilke M, de Jonge H (2006) Cellular and animal models of cystic fibrosis, tools for drug discovery. Drug Discov Today Dis Model 3:251–259. https://doi.org/10.1016/j.ddmod.2006.09.003
31. Myerburg MM, Latoche JD, Mckenna EE et al (2007) Hepatocyte growth factor and other fibroblast secretions modulate the phenotype of human bronchial epithelial cells. Lung Cell Mol Physiol 292:1352–1360. https://doi.org/10.1152/ajplung.00328.2006
32. Martinovich KM, Iosifidis T, Buckley AG et al (2017) Conditionally reprogrammed primary airway epithelial cells maintain

morphology, lineage and disease specific functional characteristics. Sci Rep 7:1–13. https://doi.org/10.1038/s41598-017-17952-4
33. Harvey PR, Tarran R, Garoff S, Myerburg MM (2011) Measurement of the airway surface liquid volume with simple light refraction microscopy. Am J Respir Cell Mol Biol 45:592–599. https://doi.org/10.1165/rcmb.2010-0484OC
34. Markovetz MR (2017) Multiscale mathematical modeling of the absorptive and mucociliary pathophysiology of cystic fibrosis lung disease. PhD Diss
35. Matsui H, Davis CW, Tarran R, Boucher RC (2000) Osmotic water permeabilities of cultured, well-differentiated normal and cystic fibrosis airway epithelia. J Clin Investig 105:1419–1427
36. Goldman DE (1943) Potential, impedance, and rectification in membranes. J Gen Physiol. https://doi.org/10.1085/jgp.27.1.37
37. Danahay H (2005) Membrane capacitance and conductance changes parallel mucin secretion in the human airway epithelium. AJP Lung Cell Mol Physiol 290:L558–L569. https://doi.org/10.1152/ajplung.00351.2005
38. Zhang LA, Urbano A, Clermont G et al (2018) APT-MCMC, a C++/Python implementation of Markov Chain Monte Carlo for parameter identification. Comput Chem Eng 110:1–12. https://doi.org/10.1016/j.compchemeng.2017.11.011
39. Goodman J, Weare J (2010) Ensemble samplers with affine invariance. Commun Appl Math Comput Sci 5:65–80
40. Hogg JS (2013) Advances in rule-based modeling: compartments, energy, and hybrid simulation, with application to sepsis and cell signaling. Dissertation, p 260
41. Gupta S, Hainsworth L, Hogg J, et al (2018) Evaluation of parallel tempering to accelerate bayesian parameter estimation in systems biology. Proceedings of the 26th Euromicro International Conference on Parallel, Distributed and Network-based Process PDP, pp 690–697. https://doi.org/10.1109/pdp2018.2018.00114
42. Pressly MA, Neal MD, Clermont G, Parker RS (2017) Dynamic Modeling of Thromboelastography To Inform State of Coagulopathy in Trauma Patients. In: Conference Paper 105 for the Foundations of Computer Aided Process Operations/Chemical Process Control Conference. Tuscan, AZ
43. Willumsen NJ, Boucher RC (1991) Sodium transport and intracellular sodium activity in cultured human nasal epithelium. Am J Physiol 261:C319–C331
44. Willumsen NJ, Boucher RC (1991) Transcellular sodium transport in cultures cystic fibrosis human nasal epithelium. Am J Physiol 30:C332–C341
45. Strieter J, Stephenson JL, Palmer LG, Weinstein M (1990) Volume-activated chloride permeability can mediate cell volume regulation in a mathematical model of a tight epithelium. J Gen Physiol 96:319–344. https://doi.org/10.1085/jgp.96.2.319
46. Matsui H, Davis CW, Tarran R, Boucher RC (2000) Osmotic water permeabilities of cultured, well-differentiated normal and cystic fibrosis airway epithelia. J Clin Invest 105:1419–1427. https://doi.org/10.1172/JCI4546
47. Willumsen NJ, Boucher RC (1991) Transcellular sodium transport in cultured cystic fibrosis human nasal epithelium. Am J Physiol 261:C332–C341
48. Donaldson SH, Bennett WD, Zeman KL et al (2006) Mucus clearance and lung function in cystic fibrosis with hypertonic saline. N Engl J Med 354:241–250. https://doi.org/10.1056/NEJMoa043891
49. Hasler U (2005) Dual effects of hypertonicity on aquaporin-2 expression in cultured renal collecting duct principal cells. J Am Soc Nephrol 16:1571–1582. https://doi.org/10.1681/ASN.2004110930
50. Zhou B, Ann DK, Li X et al (2006) Hypertonic induction of aquaporin-5: novel role of hypoxia-inducible factor-1. AJP Cell Physiol 292:C1280–C1290. https://doi.org/10.1152/ajpcell.00070.2006
51. Bertrand CA, Zhang R, Pilewski JM, Frizzell RA (2009) SLC26A9 is a constitutively active, CFTR-regulated anion conductance in human bronchial epithelia. J Gen Physiol 133:421–438. https://doi.org/10.1085/jgp.200810097
52. Lee RJ, Foskett JK (2014) Ca^{2+} signaling and fluid secretion by secretory cells of the airway epithelium. Cell Calcium 55:325–336. https://doi.org/10.1016/j.ceca.2014.02.001
53. Zuo P, Picher M, Okada SF et al (2008) Mathematical model of nucleotide regulation on airway epithelia: implications for airway homeostasis. J Biol Chem 283:26805–26819. https://doi.org/10.1074/jbc.M801516200
54. Garcia GJM, Picher M, Zuo P et al (2011) Computational model for the regulation of extracellular ATP and adenosine in airway epithelia. Springer, Dordrecht, pp 51–74
55. Donaldson SH, Boucher RC (1998) Therapeutic applications for nucleotides in lung disease BT. In: Turner JT, Weisman GA, Fedan JS (eds) The P2 nucleotide receptors. Humana Press, Totowa, NJ, pp 413–424
56. Yu D, Weber CR, Shen L et al (2011) Tight junction pore and leak pathways: a dynamic duo. Annu Rev Physiol 73:283–309. https://doi.org/10.1146/annurev-physiol-012110-142150
57. Cystic Fibrosis Foundation (CFF) (2017) 2017 Patient Registry: Annual Data Report
58. Donaldson SH, Corcoran TE, Laube BL, Bennett WD (2007) mucociliary clearance as an outcome measure for cystic fibrosis clinical research. Proc Am Thorac Soc 4:399–405. https://doi.org/10.1513/pats.200703-042BR
59. Corcoran TE, Huber AS, Myerburg MM et al (2019) Multiprobe nuclear imaging of the cystic fibrosis lung as a biomarker of therapeutic effect. J Aerosol Med Pulm Drug Deliv. https://doi.org/10.1089/jamp.2018.1491
60. Hoffman LR, Ramsey BW (2013) Cystic fibrosis therapeutics: the road ahead. Chest 143:207–213. https://doi.org/10.1378/chest.12-1639
61. Elkins MR, Sc MH, Robinson M et al (2006) A controlled trial of long-term inhaled hypertonic saline in patients with cystic fibrosis. New Engl J 354:229–240
62. Chiesi (2019) Bronchitol for management of cystic fibrosis in adult patients pulmonary-allergy drugs advisory committee meeting datE: May 8, 2019 Advisory Committee briefing materials
63. Burness CB, Keating GM (2012) Mannitol dry powder for inhalation. Drugs 72:1411–1421. https://doi.org/10.2165/11208950-000000000-00000
64. Bilton D, Tino G, Barker AF et al (2014) Inhaled mannitol for non-cystic fibrosis bronchiectasis: a randomised, controlled trial. Thorax. https://doi.org/10.1136/thoraxjnl-2014-205587
65. Robinson M, Daviskas E, Eberl S et al (1999) The effect of inhaled mannitol on bronchial mucus clearance in cystic fibrosis patients: a pilot study. Eur Respir J 14:678–685. https://doi.org/10.1034/j.1399-3003.1999.14c30.x
66. Nichols DP, Durmowicz AG, Field A et al (2019) Developing inhaled antibiotics in cystic fibrosis: current challenges and opportunities. Ann Am Thorac Soc 16:534–539. https://doi.org/10.1513/annalsats.201812-863ot
67. Agent P, Parrott H (2015) Inhaled therapy in cystic fibrosis: agents, devices and regimens. Breathe 11:111–118. https://doi.org/10.1183/20734735.021014